ARTICLE IN PRESS

Available online at www.sciencedirect.com

ScienceDirect

Solar Energy xxx (2010) xxx–xxx

SOLAR ENERGY

www.elsevier.com/locate/solener

Spatial disaggregation of satellite-derived irradiance using a high-resolution digital elevation model

José A. Ruiz-Arias [a,*], Tomáš Cebecauer [b,c,d], Joaquín Tovar-Pescador [a], Marcel Šúri [b,c]

[a] *Department of Physics, University of Jaén, Spain*
[b] *European Commission, Joint Research Centre, Ispra, Italy*
[c] *GeoModel s.r.o., Bratislava, Slovakia*
[d] *Institute of Geography, Slovak Academy of Sciences, Bratislava, Slovakia*

Received 10 February 2009; received in revised form 20 April 2010; accepted 6 June 2010

Communicated by: Associate Editor David Renne

Abstract

Downscaling of the Meteosat-derived solar radiation (∼5 km grid resolution) is based on decomposing the global irradiance and correcting the systematic bias of its components using the elevation and horizon shadowing that are derived from the SRTM-3 digital elevation model (3 arc sec resolution). The procedure first applies the elevation correction based on the difference between coarse and high spatial resolution. Global irradiance is split into direct, diffuse circumsolar and diffuse isotropic components using statistical models, and then corrections due to terrain shading and sky-view fraction are applied. The effect of reflected irradiance is analysed only in the theoretical section. The method was applied in the eastern Andalusia, Spain, and the validation was carried out for 22 days on April, July and December 2006 comparing 15-min estimates of the satellite-derived solar irradiance and observations from nine ground stations. Overall, the corrections of the satellite estimates in the studied region strongly reduced the mean bias of the estimates for clear and cloudy days from roughly 2.3% to 0.4%.

Keywords: Solar irradiance; Satellite; Digital elevation model; DEM; Disaggregation

1. Introduction

Efficient planning and operation of solar energy systems require site- and time- specific knowledge of solar resource at high accuracy. Factors controlling the spatial and time distribution of solar radiation at global to regional scales are well described by operational satellite algorithms (Perez et al., 2002; Hammer et al., 2003; Rigollier et al., 2004; Müller et al., 2004, etc.). However, under complex terrains, irradiance estimates show systematic deviations compared to ground measurements due to terrain-related effects such as elevation gradient, obstruction and shadowing by the horizon and ground reflectance.

Influence of terrain features was already described by many authors (e.g. Dozier and Frew, 1990; Tovar et al., 1995; Dubayah and Loechel, 1997; Remund et al., 1998; Oliphant et al., 2003; Cebecauer et al., 2007). Terrain shadowing was already implemented in solar radiation models integrated within a Geographical Information System (GIS), such as *r.sun* (Šúri and Hofierka, 2004) or SRAD (Moore et al., 1993; Wilson and Gallant, 2000). However, these models use simplified atmospheric parametrizations based on lumped regional parameters and their use for operational modelling is limited (Ruiz-Arias et al., 2009).

Terrain effects have not been thoroughly analysed yet, and they are not considered sufficiently in the present satellite operational schemes. Based on a thorough analysis we propose a disaggregation method of the estimates of satellite-derived horizontal irradiance calculated with a spatial

* Corresponding author. Tel.: +34 953212474; fax: +34 953212838.
E-mail address: jararias@ujaen.es (J.A. Ruiz-Arias).

0038-092X/$ - see front matter © 2010 Elsevier Ltd. All rights reserved.
doi:10.1016/j.solener.2010.06.002

resolution of 3 arc min (cell size ~ 5 km) considering the terrain information derived from the 3 arc sec digital elevation model (DEM, cell size ~ 90 m). The method was evaluated in the region of Andalusia, Spain.

2. Terrain effects

Complex terrain introduces significant variations in the local micro-climate. The first factor of variability is the elevation. Under similar atmospheric turbidity, the total radiative attenuation at low elevation is bigger compared to the high elevation. In a cloudless Rayleigh atmosphere, ozone and uniformly mixed gases are mainly located in the upper layers with water vapour immediately below and the aerosols in the lower layer (Gueymard, 1998). While major absorbents, water vapour and aerosols, are particularly variable over the time, combined with changes in elevation may significantly influence spatial pattern of attenuation.

Diverse illuminance angles are source of large irradiance variability (Dubayah et al., 1989, 1990), and surrounding terrain configuration influences the total amount of received irradiance by horizon shadowing, sky interception and ground reflectance. For illuminance angles greater than $\pi/2$, the surface is self-shaded (behind its own horizon) and the solar irradiance is entirely composed of diffuse irradiance.

2.1. Elevation

The coarse resolution of the satellite grid cell (~5 km) may include internal elevation differences of more than 1000 meters in some regions. The vertical gradient of global irradiance is determined mainly by the beam irradiance and the change in the optical path length Δm, assuming constant the attenuative radiative properties of the atmosphere between the two extreme elevations within the grid cell. The change in the optical path length is $\Delta m = \Delta z \cos\theta_z$ (Fig. 1) if the Earth's curvature is not considered, where Δz and θ_z are the elevation change and solar zenith angle. The beam broadband irradiance B can be approximated, according to the Bouguer–Beer–Lambert law, as:

$$B = S_0 e^{-\kappa m}, \tag{1}$$

where S_0 is the extraterrestrial irradiance, and κ is the broadband attenuation coefficient. Therefore, according to Fig. 1, if $(B_A - B_B)/B_A \sim \Delta B/B$, where B_A and B_B is the beam irradiance in the points A and B, and $m_B = m_A + \Delta z \cos\theta z$ we can write:

$$\frac{\Delta B}{B} \sim 1 - e^{-\kappa\Delta z \cos\theta_z}. \tag{2}$$

This expression shows that beam irradiance should increase exponentially with altitude, given κ constant. Furthermore, according to Eq. (2), the change of irradiance is maximum when the sun is at the zenith and zero when the sun is at the horizon, assuming the Earth's curvature as negligible.

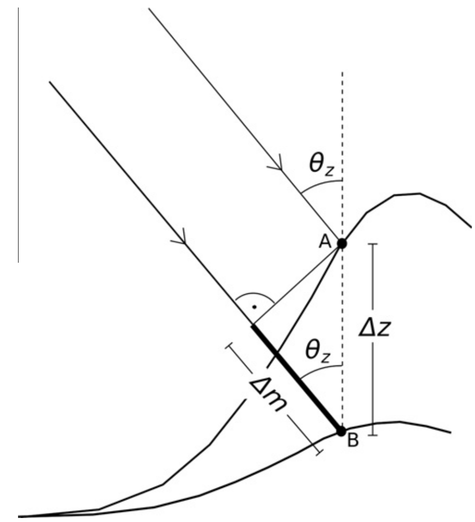

Fig. 1. Change of the optical path length Δm produced by a change of elevation Δz.

Satellite grid cell represents the spatial-time average irradiance, and let us assume the distribution of terrain elevation within the grid cell $\Phi(z)$. Let z_0 be the elevation at the satellite grid resolution. The global irradiance $G(z)$ within the grid cell can be described as a Taylor's expansion in the nearby of z_0 as:

$$G(z) = G(z_0) + \sum_{n=1}^{\infty} \frac{1}{n!} \left.\frac{\partial^n G}{\partial z^n}\right|_{z=z_0} (z - z_0)^n, \tag{3}$$

where the Taylor's remainder has been neglected. Assuming the variability of atmospheric properties negligible along the grid cell and rejecting other terrain effects, the average global irradiance in a grid cell, given the distribution of elevations and Eq. (3) is:

$$\begin{aligned}\bar{G} &= \int_{z_{\min}}^{z_{\max}} G(z)\Phi(z)dz \\ &= G(z_0) + \sum_{n=1}^{\infty} \frac{1}{n!} \left.\frac{\partial^{(n)} G}{\partial z^{(n)}}\right|_{z=z_0} \int_{z_{\min}}^{z_{\max}} (z - z_0)^n \Phi(z)dz,\end{aligned} \tag{4}$$

where $\Phi(z)$ is normalized to the unity. The integral in the right term is the nth moment of the elevations distribution $\Phi(z)$ centred in the average value z_0. Assuming $E[z] = z_0$ for the grid cell, the first moment ($n = 1$) is zero and the second moment ($n = 2$) is the variance of z, VAR[z]. As first approximation, $n = \{1, 2\}$, the mean global irradiance can be written as function of the elevation distribution within the grid cell:

$$\bar{G} \sim G(z_0) + \frac{1}{2} \left.\frac{\partial^2 G}{\partial z^2}\right|_{z=z_0} \mathrm{VAR}[z]. \tag{5}$$

Therefore, the satellite irradiance at every grid cell should show a linear dependency with the intra-grid cell variability of the elevation, being the irradiance at the average elevation $G(z_0)$ the intercept of the curve. To verify this expression, Fig. 2 shows the intra-grid cell elevation variance against the satellite grid solar irradiance estimate the July 3rd at 12:00 h (cloudless situation) when the sun is at the zenith and, according to Eq. (2), the effect of the elevation variability is the highest. The small slope of the fitting curve points out that although the dependence exists, it is actually weak.

2.2. Terrain configuration effects

Global irradiance at the surface consists of the beam and diffuse irradiances, the latter being the sum of the isotropic and the circumsolar components. The contribution of the horizon band (as a result of higher optical air-mass) is also considered by some authors (Perez et al., 1986, 1990a), however, we did not consider this component as it is permanently blocked or reduced by the surrounding terrain. Terrain reflectance can be occasionally important source of diffuse irradiance in mountains, especially in snow conditions.

2.2.1. Terrain shadowing

The spatial configuration of the surrounding terrain controls the distribution of the beam and diffuse circumsolar irradiances at low sun altitudes through the local horizon. In such a case, only isotropic diffuse irradiance reaches the ground surface. Fig. 3 compares ground measurements affected by shading episodes at sunrise and sunset with the estimates of a clear-sky model without terrain parametrization.

The horizon angle in a given direction is defined as the angle between the horizontal plane and the upper edge of elevated terrain in that direction. The algorithms to calculate horizon angles from the DEM are published in Dozier and Frew (1990) or Hofierka et al. (2007). Mathematically, the presence of shadowing can be described by the discrete Heaviside step function, $H(x)$, defined as 0 when x is negative, 1/2 when x is zero and 1 otherwise. If we note as $\alpha_S^{\phi_s}$ the solar altitude (with ϕ_s the sun's azimuth) and as $\alpha_H^{\phi_s}$ the terrain horizon angle in the azimuthal direction ϕ_s,

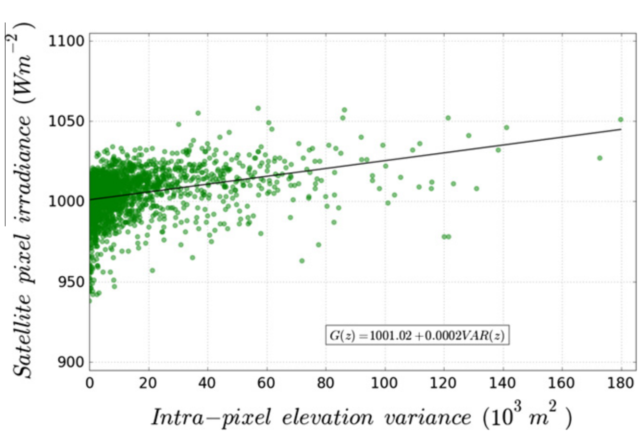

Fig. 2. Satellite irradiance against the intra-grid cell elevation variance for the 3rd July 2006 at 12:00 h (clear sky situation) for the entire study region (Fig. 4).

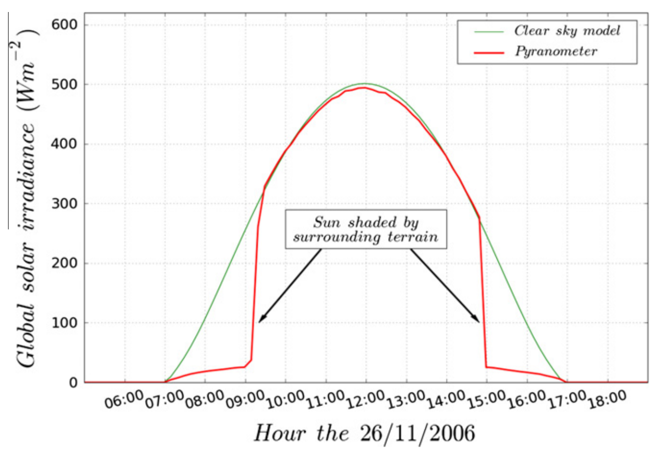

Fig. 3. Measured global irradiance (red line), affected by horizon, and the estimate of a clear-sky model without shadowing (green line). (For interpretation of the references to color in this figure legend, the reader is referred to the web version of this article.)

the shadowing-correction of the beam and diffuse circumsolar irradiances is given by:

$$\hat{B} = H(\alpha_S^{\phi_s} - \alpha_H^{\phi_s})B, \tag{6}$$

$$\hat{D}_c = H(\alpha_S^{\phi_s} - \alpha_H^{\phi_s})D_c, \tag{7}$$

where $\hat{B}$ and B are, respectively, the shadowing-corrected and uncorrected beam irradiances and $\hat{D}_c$ and D_c the shadowing-corrected and uncorrected circumsolar diffuse irradiances. The case of the self-shading, when the illuminance angle is greater than $\pi/2$, is included in this correction. When the horizon angle and the sun zenith angle are the same, the Heaviside function takes the value 1/2.

2.2.2. Sky obstruction

Similarly to the beam and diffuse circumsolar irradiances, the isotropic diffuse irradiance D_i can be also partially blocked by the surrounding terrain that reduce the effective portion of the sky dome from where the irradiance reaches the target site. Unlike the beam and circumsolar diffuse shadowing, the sky obstruction is permanent.

The amount of isotropic diffuse irradiance obscured by the terrain is estimated by the sky view factor V_d, defined as the ratio of the diffuse sky irradiance at a point to that on an unobstructed horizontal surface, i.e. $0 < V_d \leqslant 1$. According to Dozier and Frew (1990), the sky view factor for a surface with slope S and azimuth A can be approximated as:

$$V_d \approx \frac{1}{2\pi}\int_0^{2\pi}\left[\cos S\sin^2 H_\phi + \sin S\cos(\phi - A)\right.$$
$$\left.\times\left(H_\phi - \sin H_\phi\cos H_\phi\right)\right]d\phi, \tag{8}$$

where H_ϕ is the angle from zenith to horizon in the azimuthal direction ϕ. The horizon zenith angle integrates both the terrain horizon and the horizon imposed by the inclined surface and it is calculated as the minimum of these two in a given azimuthal direction. Note that

Eq. (8) assumes the important simplification of a completely isotropic sky dome. In the particular case of a horizontal surface,

$$V_d \approx \frac{1}{2\pi}\int_0^{2\pi} \sin^2 H_\phi d\phi, \tag{9}$$

and, with an uniform sampling of the horizon angle in N directions around the target site, in the discrete case, we have:

$$V_d \approx \frac{1}{N}\sum_{i=1}^{N} \sin^2 H_{\phi,i}. \tag{10}$$

Finally, using the sky view factor, the corrected isotropic diffuse irradiance $\hat{D}_i$ can be calculated as:

$$\hat{D}_i = V_d D_i. \tag{11}$$

2.2.3. Terrain reflectance

In mountains, the reflected diffuse irradiance R from the surrounding terrain can be sometimes important. It depends on the terrain configuration and, typically, is difficult to model. Therefore, it is assumed to have an isotropic behaviour and approximated by the terrain configuration factor C_t for an infinitely long slope:

$$C_t \approx \frac{1+\cos S}{2} - V_d. \tag{12}$$

For a horizontal surface, $C_t \approx 1 - V_d$ (Dozier and Frew, 1990; Siegel and Howell, 1981).

Then, the reflected diffuse irradiance can be calculated as:

$$R = \rho C_t\left[\hat{B} + \hat{D}_c + (1 - V_d)D_i\right], \tag{13}$$

where ρ is the ground albedo. The factor $1 - V_d$ scales the isotropic diffuse irradiance to that coming just from the terrain-obstructed portion of the sky dome.

Finally, the total global irradiance at the horizontal surface corrected for terrain effects can be calculated as $\hat{G} = \hat{B} + \hat{D}_c + \hat{D}_i + R$.

3. Study area

The method was applied to the eastern Andalusia area, Spain (Fig. 4), covering around 230 × 245 km^2. The region includes the mountainous systems of Sierra Nevada and Sierra Mágina, the National Park of Cazorla, Segura y Las Villas and, partly, also the Guadalquivir river basin flat area. The fine resolution DEM was extracted from the SRTM-3 data (Farr et al., 2007) that was also averaged to the grid resolution of the satellite (3 arc min).

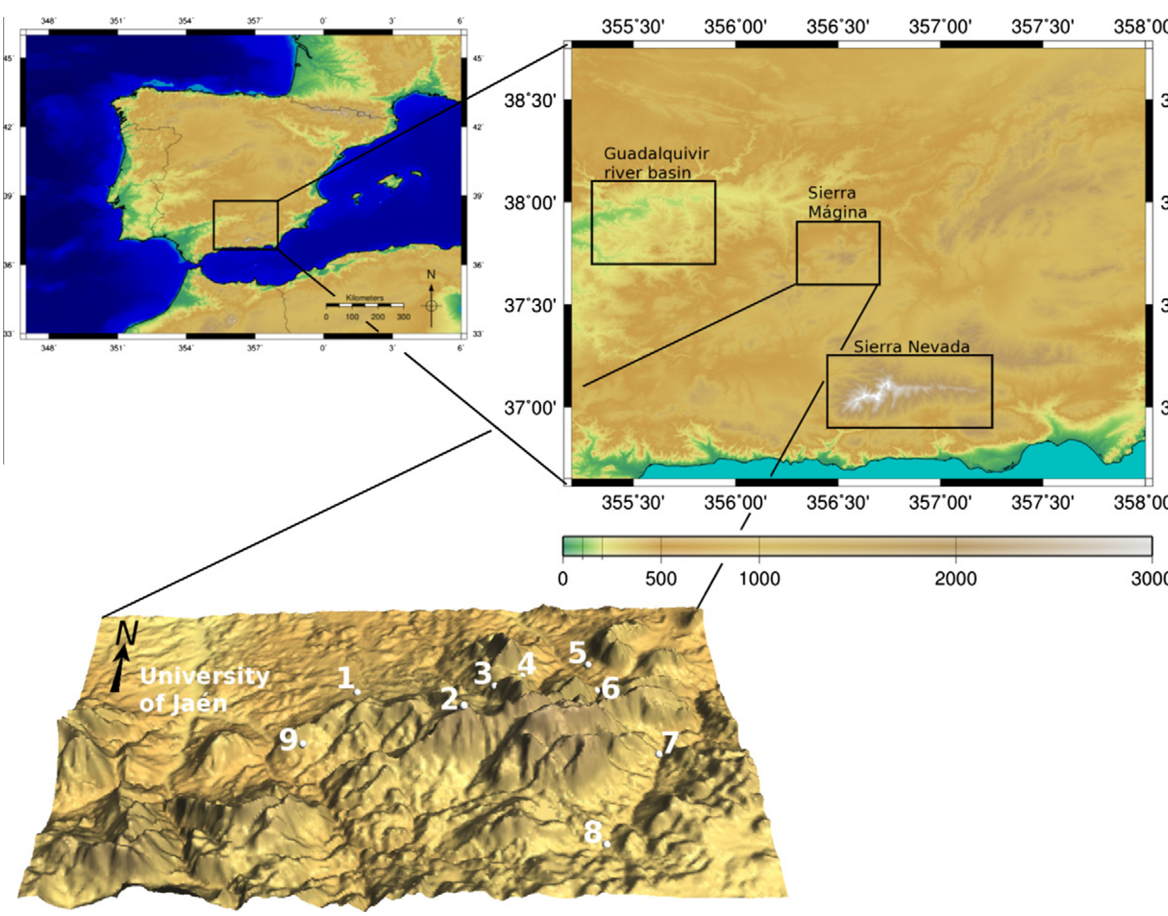

Fig. 4. Study area in Andalusia, Spain. Distribution of the radiometric stations in the Natural Park of Sierra Mágina, Jaén.

Please cite this article in press as: Ruiz-Arias, J.A. et al. Spatial disaggregation of satellite-derived irradiance using a high-resolution digital elevation model. Sol. Energy (2010), doi:10.1016/j.solener.2010.06.002

3.1. Ground data

The validation was carried out using observations from nine radiometric stations (Table 1) deployed in the Natural Park of Sierra Mágina. The stations are equipped with HOBO (Onset Corporation) data-loggers recording global irradiance registered by Licor 200-SZ radiometers. The instrumental error is estimated to be less than 5%, typically 3%. The data are recorded in a 10-min step in seven stations, and in a 5-min step for two of the stations. For this work, the data were linearly interpolated to a 15-min step to match the satellite time sampling.

3.2. Satellite-derived irradiance

The algorithm to derive solar irradiance from geostationary satellite data is based on the approach proposed by Verdebout (2000, 2004). The calculation scheme, originally developed for UV irradiance, was adapted for calculation of shortwave radiation from Meteosat Second Generation (MSG) satellite data. According to this scheme the surface irradiation is obtained by interpolation of multidimensional look up table (LUT) relating surface irradiance to a set of input parameters. The LUT was generated using the radiative transfer code libRadtran v1.3 (Mayer and Kylling, 2005) for a variety of atmospheres and cloud conditions described by total ozone column amount, near surface horizontal visibility, effective surface albedo, cloud optical thickness and atmospheric water vapour. The horizontal visibility was used to approximate the atmospheric optical depth and was derived on daily basis from 1000 meteorological stations over Europe. The variability of water vapour was simplified to a constant value. In addition to these parameters, the LUT also describes the surface irradiance for a range of surface elevations and solar zenith angles.

The cloud optical thickness as an estimate of the radiation attenuation by clouds was derived from MSG data using a second LUT that simulates the "at sensor radiance". The actual cloud optical thickness was calculated by inversion of the LUT, and interpolating between the pre-calculated values for the actual image digital count, the effective surface albedo and the solar and satellite geometry. In this approach, the lowest value in 10-days image stack was used to calculate effective surface albedo for snow-free pixel. The algorithm also accounts for the reverse response of the image digital counts to increase cloud thickness at pixels with high effective surface albedo, e.g. snow. For the snow detection algorithm, additional spectral bands from the middle infrared and thermal bands of the MSG instruments were used. Further details about retrieval of surface irradiance from satellite data can be found in Verdebout (2000, 2004).

The results of this model were layers of shortwave irradiance with spatial resolution of 3 arc min in 15 min time step.

4. Method

Fig. 5 shows a general schema of the proposed disaggregation method. In the first step, the elevation is corrected by enhancing the satellite resolution (3 arc min, ~5 km at mid-latitudes) to the resolution of 3 arc sec (~90 m at mid-latitudes). This correction mainly affects the beam irradiance and is only applied in those grid cells that represent cloudless conditions, the criterion being the air-mass corrected clearness index (Perez et al., 1990b) above 0.65. After the disaggregation step, the global irradiance is decomposed into direct and diffuse (circumsolar and isotropic) components. The diffuse component and its fractions are estimated using the regressive model of Ruiz-Arias et al. (2010) and the Perez model (Perez et al., 1990a). Finally, the terrain corrections were applied and the components summed up to yield the terrain-corrected high-resolution global irradiance.

4.1. Elevation correction

The vertical profile of global irradiance was determined by the change of the optical path length. Fig. 6a shows the vertical profile calculated with the ESRA clear-sky model (Rigollier et al., 2000) using a Linke turbidity at sea level of 3.5 and a sun altitude of 30°. It can be seen that although in relative terms the decrease of the diffuse irradiance is close to 50%, in absolute terms it is the direct irradiance who drives the change.

Two different approaches to parametrize the vertical profile of solar irradiance were evaluated: parametrization

Table 1
Location, geographical coordinates (decimal degrees; North and East positive), elevation and sky-view fraction of the Sierra Mágina's stations network. Altitude is given in meters above sea level.

Id	Location	Latitude	Longitude	Altitude (measured)	Altitude (3 arc min DEM)	Altitude (3 arc sec DEM)	Sky-view fraction
1	Mancha Real	37.785	−3.612	762	840	759	0.99
2	Peak Almadén	37.734	−3.527	1982	1423	2014	0.98
3	Torres	37.780	−3.498	1075	1158	1102	0.96
4	Albanchez	37.795	−3.473	864	1158	930	0.91
5	Bedmar	37.815	−3.413	634	590	642	0.97
6	Virgen de Cuadros	37.789	−3.410	603	1028	629	0.91
7	Bélmez	37.727	−3.370	704	894	781	0.98
8	Huelma	37.653	−3.424	859	1000	876	0.98
9	Pegalajar	37.738	−3.655	791	635	828	0.97

Please cite this article in press as: Ruiz-Arias, J.A. et al. Spatial disaggregation of satellite-derived irradiance using a high-resolution digital elevation model. Sol. Energy (2010), doi:10.1016/j.solener.2010.06.002

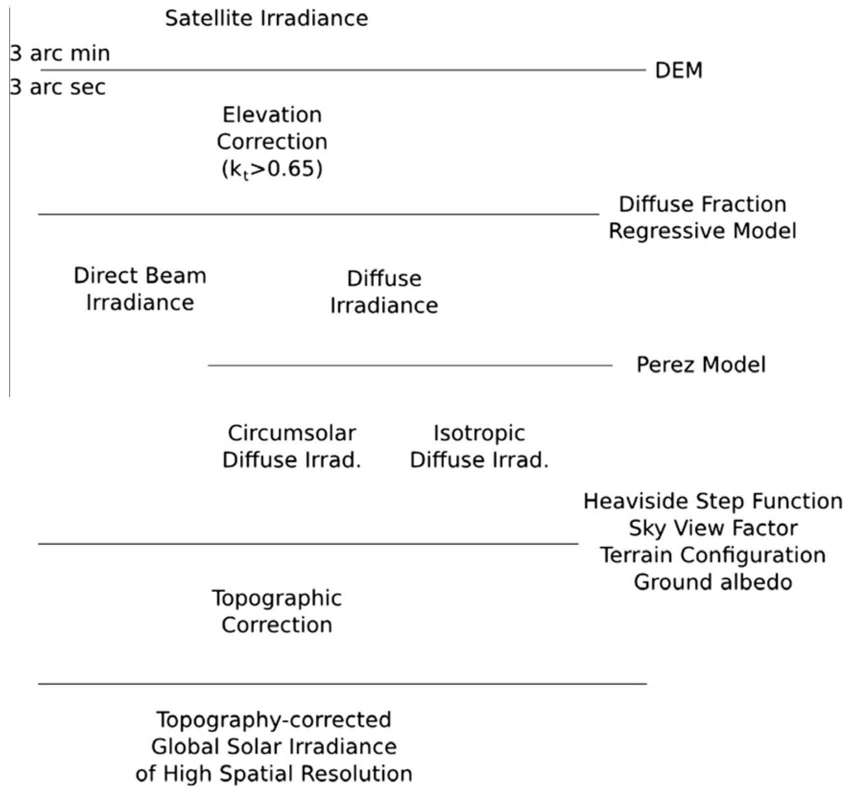

Fig. 5. Schema of the disaggregation method.

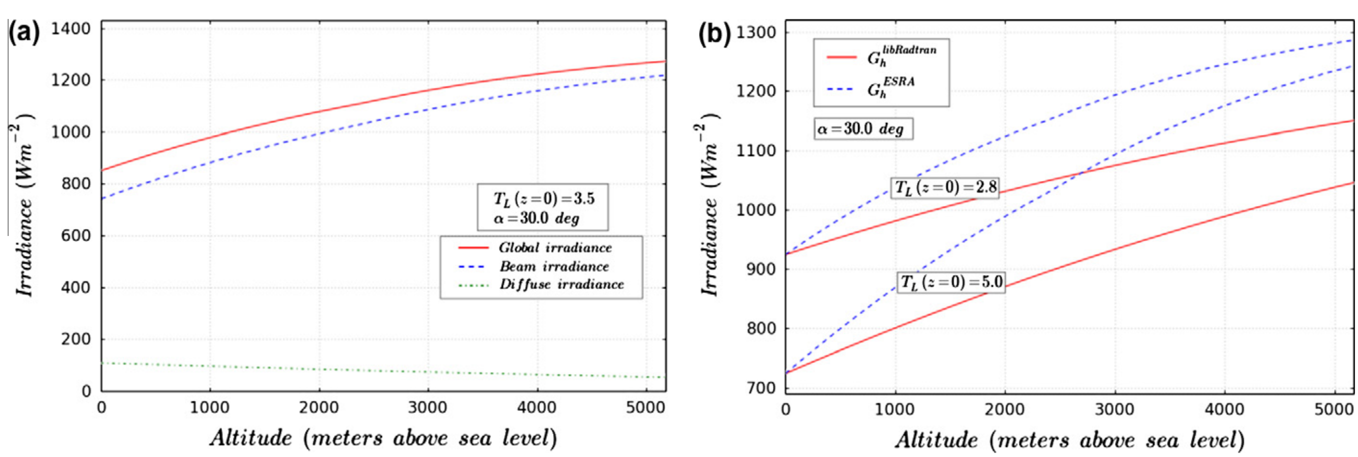

Fig. 6. (a) Vertical profile of global irradiance and its components according to the ESRA clear-sky model for Linke turbidity of 3.5 at sea level and solar altitude 30°. (b) Comparison of the global irradiance vertical profile for two different Linke turbidities (2.8 and 5.0) using ESRA clear-sky model, and the fitting function proposed by Oume and Wald based on the libRadtran radiative transfer.

based on the ESRA model and the fitting function proposed by Abdel Wahab et al. (2008) (see also Oumbe and Wald, 2010). The latter approach is based on simulations of the libRadtran radiative transfer code (Mayer and Kylling, 2005). The inter-comparison of the two approaches for two Linke atmospheric turbidities (2.8 and 5.0, Fig. 6b) shows stronger vertical gradient in the ESRA equations. The fitting function fits better the satellite model used in this study, presumably because it is also based on the libRadtran code.

It was designed to consider the optical turbidity of the atmosphere. For global irradiance it is given by:

$$G_c(z) = S_0 e^{-\tau(z)}, \tag{14}$$

where

$$\begin{aligned} \tau(z) &= \tau(z_0)\beta^{z_0-z}, & z < 2000 \\ \tau(z) &= \tau(z_0)\beta_1^{z_0-2}\beta_2^{2-z}, & z \geqslant 2000 \end{aligned} \tag{15}$$

and $\tau(z_0) = -\ln[G_c(z_0)/S_0]$. The parameter S_0 is the irradiance at the top of the atmosphere. For z less than 2 km,

$\beta = 1.20$. For z greater than 2 km, if T_L is greater than 5, $\beta_1 = 1.30$; otherwise, $\beta_1 = 1.20$ and $\beta_2 = 1.20$.

As this correction is only applicable to cloudless conditions, the elevation correction was only carried out on those satellite grid cells with an air-mass-corrected clearness index k_t' greater than 0.65 (Perez et al., 1990b).

4.2. Decomposition of global irradiance

The regressive model proposed by Ruiz-Arias et al. (2010) was used for decomposing into the beam and diffuse irradiances. The model was developed and validated using data of 21 stations spread over USA and Europe, including the Iberian Peninsula:

$$k_d = 0.952 - 1.041 e^{-\exp(2.300 - 4.702 k_t)}, \tag{16}$$

where k_t is the clearness index.

In spite of the high root mean square error of the model (over 30%), the re-aggregation of the solar components after the terrain corrections minimizes the potential effects of the error in the decomposition over the final terrain-corrected estimates.

4.3. Decomposition of diffuse irradiance

It has been assumed that the diffuse irradiance is the aggregation of the isotropic background and the circumsolar disk. Considering the size of the circumsolar disk negligible, it can be incorporated to the beam irradiance as the two are affected in the same way by shadowing. The isotropic component must be scaled with the sky-view fraction.

The decomposition of isotropic and circumsolar components is based on the Perez tilted diffuse model (Perez et al., 1990a) for the special case of a horizontal surface. Therefore, the circumsolar diffuse irradiance D_c is estimated as:

$$D_c = F_1 D_h, \tag{17}$$

where D_h is the diffuse irradiance and F_1 is given by:

$$F_1 = F_{11} + F_{12}\Delta + F_{13}Z, \tag{18}$$

where F_{ij} are coefficients tabulated as a function of the value of the sky's clearness, Δ is the sky's brightness and Z is the sun zenith angle. The isotropic diffuse irradiance is then:

$$D_i = D_h - D_c. \tag{19}$$

4.4. Terrain corrections

Once the components of the global irradiance have been decomposed, application of the terrain corrections is straightforward. Firstly, the beam and diffuse circumsolar irradiances are removed if the shadowing is detected (Eqs. (6) and (7)). The horizon angles were derived within the GRASS GIS framework using the *r.horizon* module (Neteler and Mitasova, 2008; Hofierka et al., 2007). Secondly, the isotropic diffuse irradiance was scaled with the sky-view fraction (Eq. (11)).

Fig. 7 illustrates the relative importance of corrections of the circumsolar and isotropic diffuse irradiance as a function of the clearness index. For clearness indices less than 0.4, the high cloud optical absorption causes that the circumsolar fraction k_c (circumsolar diffuse/global irradiance) remains smaller than 0.10 (Fig. 7a). However, for a clearness index over 0.6, it reaches its maximum value around 0.15, and for very clear conditions its value again decreases because the atmospheric scattering decreases as well. The relative importance of the shadowing correction will be higher for clear-sky conditions, as the beam component is higher.

Fig. 7b shows the relative importance of the sky obstruction correction for a sky-view fraction of 0.9. Given that diffuse fraction k_d (diffuse/global irradiance) is the sum of the circumsolar diffuse fraction k_c and the isotropic diffuse fraction k_i (isotropic diffuse/global irradiance), the relative importance of the isotropic correction is higher under

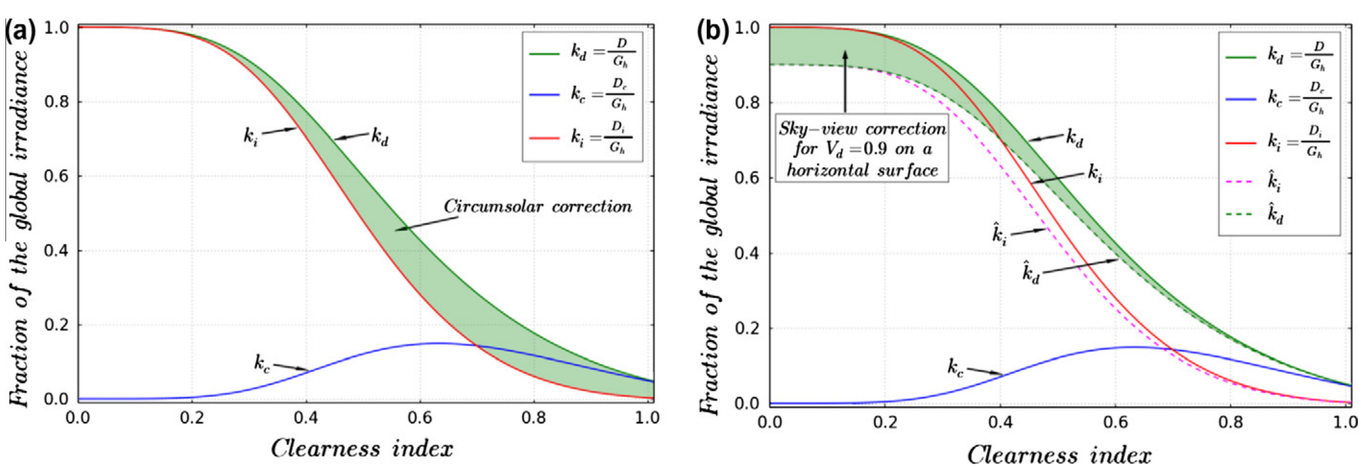

Fig. 7. (a) Relative importance of the correction of the circumsolar diffuse component shaded by a horizon as a function of the clearness index. (b) Relative importance of the sky view factor correction on the isotropic diffuse irradiance as a function of the clearness index.

Please cite this article in press as: Ruiz-Arias, J.A. et al. Spatial disaggregation of satellite-derived irradiance using a high-resolution digital elevation model. Sol. Energy (2010), doi:10.1016/j.solener.2010.06.002

overcast conditions, when the atmospheric optical extinction is higher and the diffuse irradiance is entirely isotropic. But, in absolute terms, this correction is small since under overcast conditions there is no beam component and the global irradiance is low.

The reflected diffuse irradiance is usually the smallest component of incoming irradiance, and depends also on the terrain reflectance. Because of the strong dependence on the ground albedo, it can have a noticeable relative importance in snow and ice conditions.

5. Discussion

5.1. Validation with ground data

Four time series, totalling 22 days on April, July and December 2006 were selected from the validation database of the Sierra Mágina's radiometric network. Overall, 1282 satellite-derived time frames (time step of 15 min.) were tested against this validation dataset.

To test the performance of the disaggregation methodology, we have divided the days into cloudy and cloudless days. The latter were considered as those with an average daily clearness index at stations 1, 5 and 8 greater than 0.65. Thus, we have 11 cloudy days and 11 cloudless days. Besides, we have selected three cloudless days on July and another three on April in order to test the shadowing correction for different sun altitudes.

Fig. 8 shows the mean bias error (MBE) and root mean square error (RMSE) of the satellite estimates (3 arc min resolution) and the disaggregated irradiance (3 arc sec resolution) at each radiometric station. Particularly, the disaggregation improved the MBE and RMSE at stations 3, 4 and 6, those under stronger terrain influence (Table 1). However, they get worse at the station 2, located over 2000 meters above sea level, and with environment conditions far from the rest of stations. The rest of stations do not present significant changes. This ambiguity should be mostly related to the non-null uncertainty of the terrain representation given by the DEM since under clear-sky conditions the uncertainty related to the atmosphere is lower. The same conclusions are extracted from Fig. 9, where the improvement of the disaggregated estimates is strongly dependent of the specific point under consideration and mainly driven by the terrain representation.

As shown in Fig. 4, horizon shading produces a strong drop of the measured diurnal irradiance curve at sunrise and sunset and, if the shading is not taken in account, the model will show an overestimation (Fig. 10a). However, when horizon is calculated, the DEM inaccuracies

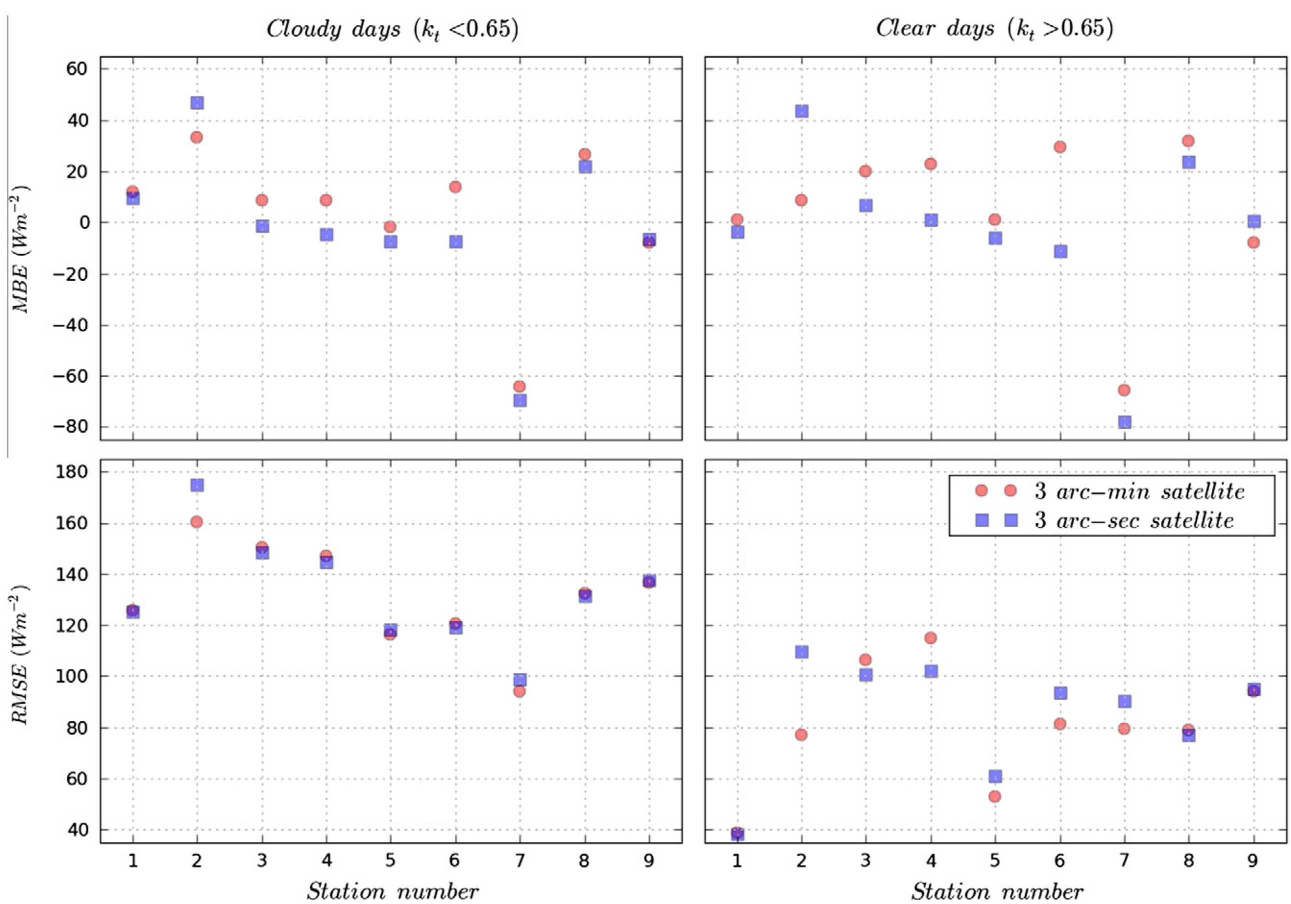

Fig. 8. Mean bias error and root mean square error for clear-sky and cloudy days for all the stations. A negative MBE means that satellite or disaggregated irradiance underestimate the ground measurements.

Please cite this article in press as: Ruiz-Arias, J.A. et al. Spatial disaggregation of satellite-derived irradiance using a high-resolution digital elevation model. Sol. Energy (2010), doi:10.1016/j.solener.2010.06.002

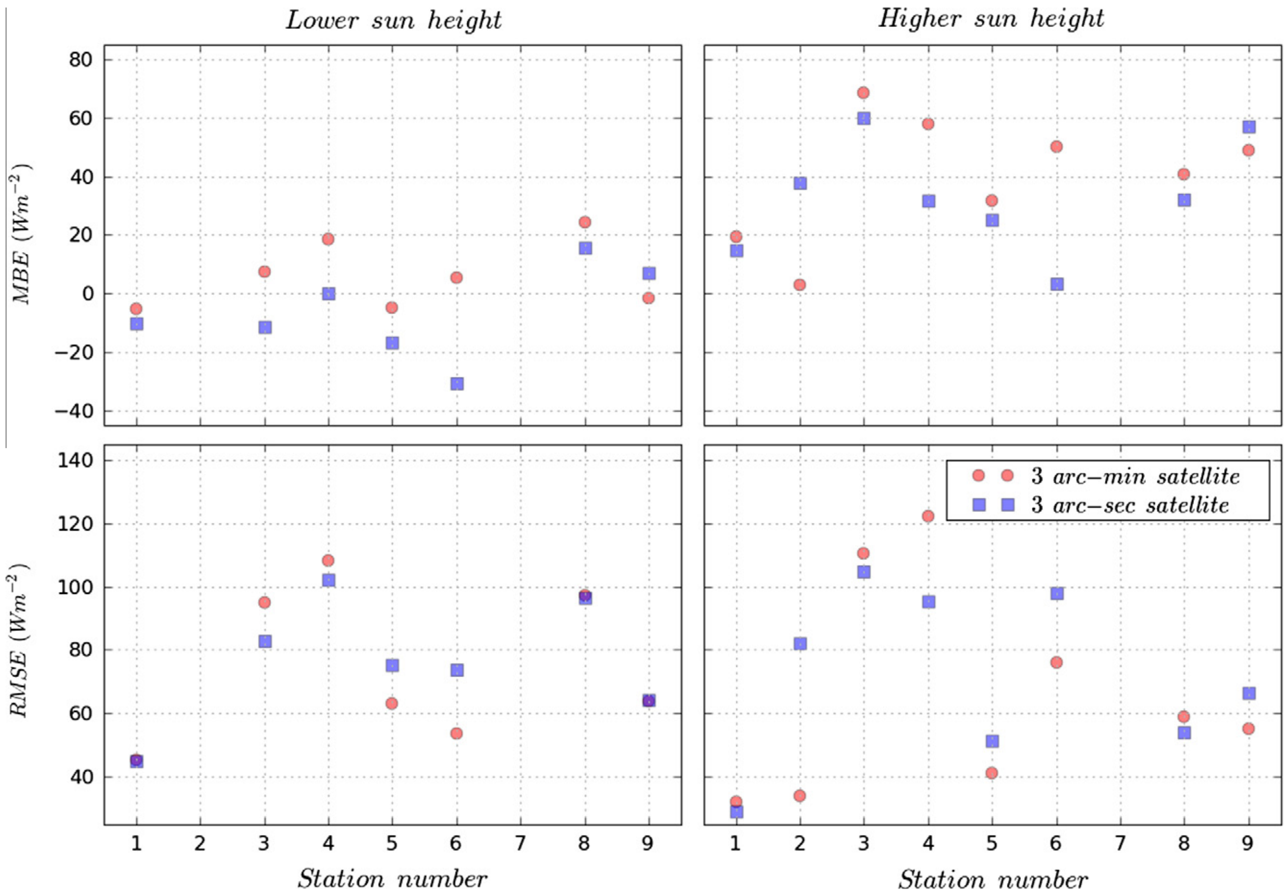

Fig. 9. Same as Fig. 8 but for clear days on April and July.

lead to misinterpret some data pairs as points under shadowing (Fig. 10b). Such errors in the horizon estimation should decrease as the quality of the DEM increases.

Table 2 presents the error analysis of the satellite and disaggregated estimates considering all the experimental stations. The analysis is presented for clear and cloudy days on April (lower sun altitude) and cloudless days on July (higher sun altitude). It was done separately for the initial irradiance dataset (satellite) and the terrain-corrected dataset (disaggregated), and for different atmospheric conditions, to isolate the benefits of the terrain correction from the initial errors in the satellite-derived irradiance, that are due to model parametrization inaccuracies and biased knowledge of the state of the atmosphere. Satellite estimates overestimate the ground measurements by ~2% both for clear and cloudy days, with a RMSE of 17% for cloudy days and 38% for clear days. A thorough look to the time series indicates that irradiance on cloudless days on April and December was underestimated whereas on July was overestimated. This could be attributed to a deficient estimate of the atmospheric turbidity. As regards the disaggregated data, for cloudy and cloudless days, they present certain improvement over the satellite estimates: the MBE was almost removed and the RMSE remains roughly unaltered. The analysis for the three cloudless days on April revealed a decrease of almost 13 Wm^{-2} (2.5%) in the MBE, but kept roughly the same in absolute value. According to Table 1, the estimates based on the 3 arc sec DEM are closer to the observed altitudes. This implies that elevation correction should change irradiance from a higher altitude to a lower altitude, that is, irradiance must decrease due to the higher optical path length for the lower altitude. This fact and the shading correction explain the decreasing of the MBE. For the cloudless days on July, the same comments are applicable. However, in this case, the elevation correction has a higher absolute importance given the higher sun altitude and atmospheric turbidity. On the contrary, the horizon correction is less important. Overall, the MBE is reduced to 8 Wm^{-2} (1.4%), slightly lower than on April.

5.2. Re-aggregation to the satellite resolution

To evaluate the magnitude of the correction, the high-resolution irradiances were re-aggregated by averaging to a cell size of 3 arc min. Following, these upscaled estimates were compared against the initial satellite estimates for three regions in Andalusia (Fig. 4). Sierra Nevada is a complex mountainous chain with the highest range of elevations and terrain roughness. The terrain depression of the Guadalquivir river basin is a flat area, with elevation changes clustered around the average. Sierra Mágina has

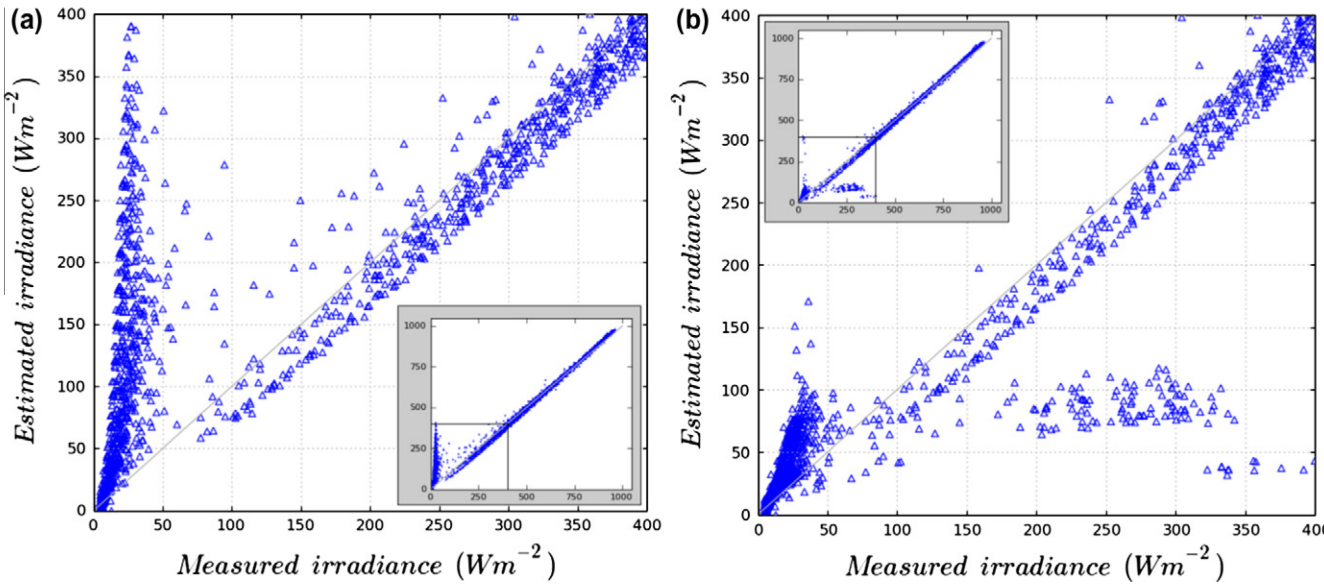

Fig. 10. Measured global irradiance at station 6 against estimated global irradiance without shadowing correction (a) and after correction (b).

Table 2
Statistical error analysis of the satellite and disaggregated estimates using all the stations in the Sierra Mágina's stations network. Negative MBE means that satellite irradiance or disaggregated irradiances underestimate the ground measurements. N is the number of test cases and r^2 the squared correlation coefficient of Pearson. Analysis is also done for days on April (low sun height) and days on July (high sun height).

	N	MBE (Wm^{-2})	rMBE (%)	RMSE (Wm^{-2})	rRMSE (%)	r^2
Satellite						
Clear days	4792	7.95	2.29	134.48	38.80	0.89704
Cloudy days	4792	11.09	2.28	84.41	17.35	0.96733
Low sun altitude	1176	6.37	1.22	78.63	15.10	0.96857
High sun altitude	1464	40.05	7.44	73.64	13.67	0.98389
Disaggregated						
Clear days	4792	1.35	0.39	135.17	39.00	0.89724
Cloudy days	4792	1.73	0.36	86.31	17.74	0.96745
Low sun altitude	1176	−6.58	−1.26	79.22	15.21	0.96854
High sun altitude	1464	32.69	6.07	76.87	14.28	0.98174

intermediate terrain roughness, not as strong as Sierra Nevada.

Statistical comparison of the upscaled satellite data with the initial estimates is detailed in Table 3 by means of the mean bias deviation (MBD), the root mean square deviation (RMSD) and their relative values (rMBD and rRMSD). A negative MBD means that the upscaled irradiance is lower than the original satellite estimate. The dataset was classified into cloudy and cloudless days and divided into two groups with sun altitude below or above 25°. Results show that terrain correction is higher for lower sun altitudes, as shadowing is more pronounced and this is relatively independent of the cloudiness. Recall that the difference in elevation for low sun altitude from the coarser to the finer resolution of the DEM is small as pointed by Eq. (2). Therefore, at high zenith angles, terrain correction is mainly driven by shadowing and sky-view fraction.

For cloudless days, the MBD ranges from −1% for the river basin sub-region to −10% for Sierra Nevada, where shadowing and sky-view fraction reduce the initial irradiance estimated from the satellite. The scattering of the correction roughly ranges from 2% to 13% for the same sub-regions. Overall, mean deviation is roughly −6.5% and the spread is over 9%. In the case of cloudy days, although the relative importance of the correction is slightly higher, the magnitude is roughly the same compared to cloudless days.

For high sun altitude, the terrain correction decreases as there are only few shadowing episodes but the relative importance of the correction due to differences in elevation increases. The correction still shows dependence with the terrain, although weaker compared to low sun altitudes. Particularly, the rMBD and rMSD after correction remain below 1% for all the regions. Under cloudy sky, both the magnitude and the relative value of the terrain correction increase over all the regions, consistently with the fact that the sky-view fraction is more significant in relative value for overcast conditions (Fig. 7b).

The terrain influence on solar radiation is not only governed by the atmospheric state, but also by the relative Sun-Earth position, in particular, by the sun altitude. The terrain dependence of the solar irradiance changes seasonally. The disaggregated irradiances upscaled to 3 arc min cell size were re-aggregated to daily estimates, and Table 4 details four clear and cloudy days on April, July and December. Both the MBD and the RMSD of the terrain-corrected irradiance are larger for December and less pronounced for July, due to the stronger shadowing. Sierra Nevada again presents the highest correction. Overall, for the whole region, the MBD and its spread are similar for

Table 3
Statistical comparison of upscaled images with the initial satellite estimates for clear and cloudy conditions. Negative MBD means that upscaled irradiances are lower than original satellite irradiances.

	Cloudy skies ($k_t' < 0.65$)				Clear skies ($k_t' \geqslant 0.65$)			
	MBD (Wm^{-2})	RMSD (Wm^{-2})	rMBD (%)	rRMSD (%)	MBD (Wm^{-2})	RMSD (Wm^{-2})	rMBD (%)	rRMSD (%)
Solar altitude < 25°								
River basin	−2.59	4.14	−3.10	4.51	−1.42	2.74	−1.09	1.90
S. Mágina	−16.38	19.62	−13.94	16.49	−15.58	19.79	−8.28	10.27
S. Nevada	−16.29	20.20	−13.95	17.29	−18.66	23.31	−10.69	12.86
All region	−6.75	10.81	−6.59	10.09	−10.44	15.27	−6.62	9.11
Solar altitude > 25°								
River basin	−0.80	1.13	−0.21	0.30	−0.06	0.53	−0.03	0.10
S. Mágina	−5.73	7.25	−1.70	2.19	−2.09	5.12	−0.60	1.09
S. Nevada	−5.74	7.53	−1.64	2.20	−0.72	3.49	−0.22	0.71
All region	−2.45	3.95	−0.64	1.08	−0.71	3.48	−0.21	0.71

Table 4
Statistical comparison of daily upscaled images with the initial daily satellite estimates for clear and cloudy conditions. Negative MBD means that upscaled irradiances are lower than original satellite irradiances.

	Cloudy skies ($k_t < 0.65$)				Clear skies ($k_t \geqslant 0.65$)			
	MBD (Wm^{-2})	RMSD (Wm^{-2})	rMBD (%)	rRMSD (%)	MBD (Wm^{-2})	RMSD (Wm^{-2})	rMBD (%)	rRMSD (%)
December								
River basin	−13.18	19.01	−0.75	1.05	−19.64	27.93	−0.84	1.19
S. Mágina	−86.59	105.01	−5.52	6.68	−164.10	201.49	−6.90	8.47
S. Nevada	−62.42	81.09	−4.61	5.88	−106.10	138.46	−5.33	6.96
All region	−40.82	62.31	−2.32	3.55	−60.67	94.45	−2.64	4.12
April								
River basin	−11.75	16.88	−0.22	0.31	−8.18	12.52	−0.13	0.20
S. Mágina	−82.34	94.67	−1.62	1.86	−77.29	89.63	−1.10	1.28
S. Nevada	−104.72	121.42	−2.71	3.14	−107.13	127.04	−1.64	1.95
All region	−45.11	67.82	−0.87	1.31	−43.18	68.02	−0.64	1.01
July								
River basin	−9.74	16.24	−0.17	0.27	−7.44	14.70	−0.09	0.18
S. Mágina	−61.99	71.00	−1.13	1.29	−66.03	77.78	−0.78	0.92
S. Nevada	−62.83	84.27	−0.96	1.27	−53.10	84.98	−0.65	1.03
All region	−31.02	48.49	−0.49	0.76	−33.47	55.33	−0.41	0.67

both clear and cloudy days: rMBD ranges from −0.5% on July to −2.5% in December and rRMSD ranges from 0.7% on July to 4% in December.

5.3. Spatial variability of the terrain effects

The availability of high-resolution maps of solar irradiances makes possible to analyse the spatial variability induced by terrain using geostatistic. Particularly, the variogram model relates the variance of a random function with the lag distance between involved points, which is itself a measure of the spatial auto-correlation of the random field. The exponential fitting function was used to derive a continuous variogram (Dubayah et al., 1990; Alsamamra et al., 2009), and it is completely characterized by three parameters: nugget, sill and range. Nugget parameter is the variance for those points separated a zero distance and is a measure of the variable continuity. The range is the spatial distance at which the variance reaches the 95% of its asymptotic value (given an exponential model) and, the variance is the sill parameter. This means that range represents the distance where the data roughly reaches the maximum variance (sill) and, above, the data is uncorrelated.

The diurnal change of the variogram for the April 26th, 2006 and July 3rd, 2006 (cloudless days) was assessed for the Guadalquivir river basin and Sierra Nevada (Fig. 11), where the range and the standard deviation are plotted. Standard deviation in Sierra Nevada is larger in these days as, otherwise, is expected. On April, its value is around 100 Wm^{-2} for the central hours of the day with some variability probably caused by marginal cast shadows. On the contrary, standard deviation of global irradiance in the river basin remains constant over 15–20 Wm^{-2} along the day. The same happens for the July 3rd, 2006, but standard deviation in Sierra Nevada decreased until ~30 Wm^{-2}. This is related to the higher sun altitude and the lack of shadows. At sunrise and sunset, the variance increases because of the occasional shadowing.

The range presents high values at sunrise and sunset (note the logarithmic y-axis scale). This means that the

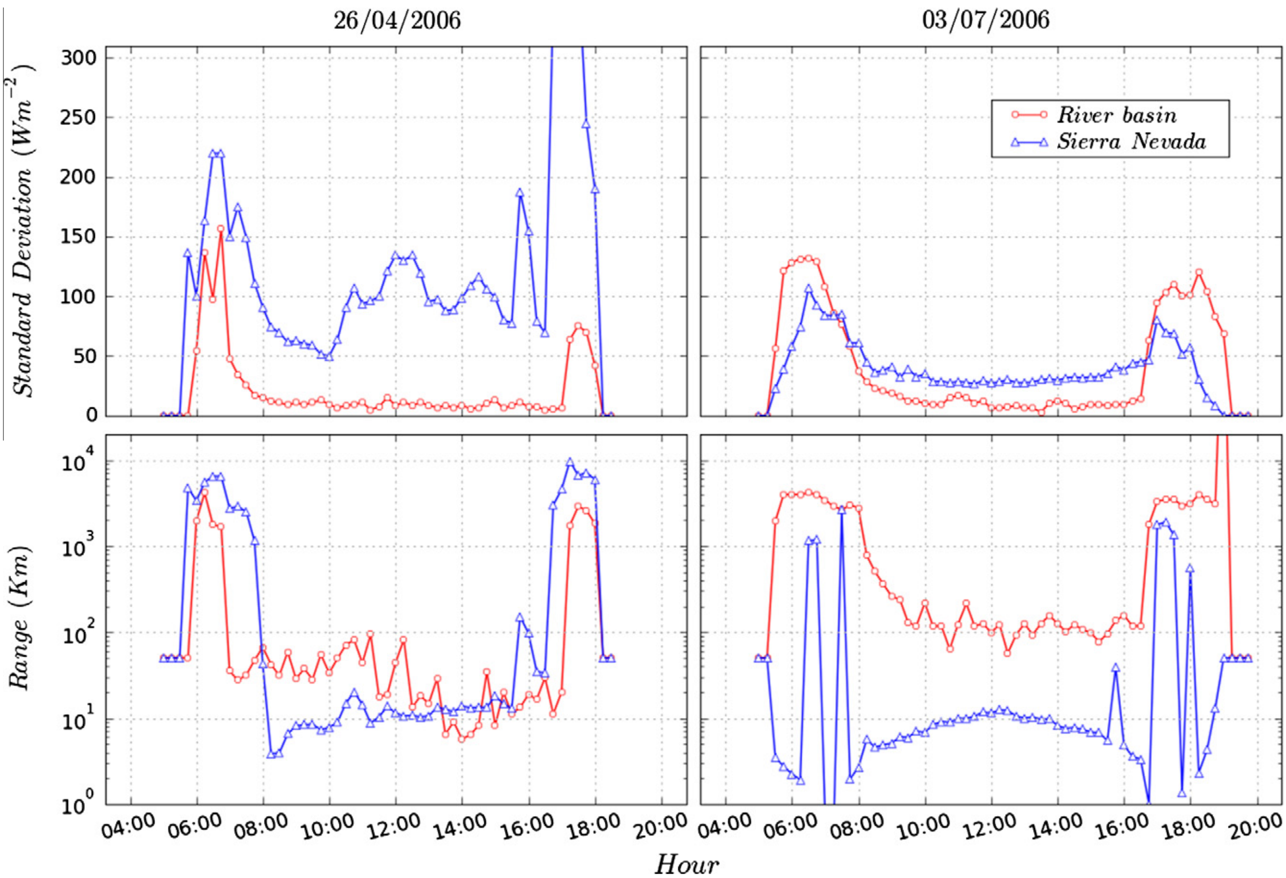

Fig. 11. Variogram for the Guadalquivir river basin and Sierra Nevada in 26/04/2006 (left column) and 03/07/2006 (right column). Upper row shows the squared root of the sill parameter (standard deviation) and lower row shows the range parameter.

spatial auto-correlation of the irradiance field is high. At these hours the optical path length is large and the direct beam irradiance is strongly attenuated. Thus, the irradiance field is relatively isotropic. Besides, the high zenith angles give rise to a scenario of generalized cast shadows over the entire region. Overall, the total irradiance field is roughly homogeneous and the spatial auto-correlation is high. As the solar altitude increases, sunlit surfaces appear and the spatial variability becomes higher. At the same time, optical path length also decreases. As a consequence, the range and the spatial auto-correlation decrease. This behaviour can be observed both for the April 3rd, 2006 and the July 3rd, 2006. It is in accordance with some previous works as those of Dubayah et al. (1990) or Essery and Marks (2007) where the authors showed that the maximum spatial variability of the irradiance field in mountainous regions is found at intermediate solar heights.

6. Uncertainties and sources of error

Along the process of disaggregation, three main sources of errors may be identified: terrain horizon inaccuracies, satellite model estimates and atmospheric parameterization.

The terrain is represented by the digital elevation model, and the increase of accuracy and grid resolution should yield better estimates of terrain horizon. As shown in Fig. 10, the inaccuracies in the horizon estimates may lead to misinterpretation in the shadowing correction. Cebecauer et al. (2007) showed that the horizon is strongly dependent of the resolution of the DEM.

The satellite-based solar radiation models used for irradiation estimates have usually limited accuracy due to the algorithmic simplifications and lack of quality inputs. To allow its operational use over larger territories, the reduced model complexity introduces errors especially in specific conditions such as broken clouds and high zenith angles. The model as described in Section 3.2 is based on the radiative transfer code with several simplified assumptions and implemented by a set of LUT tables with input parameters with higher uncertainty. As the highest occurrence of the terrain shadows is for high zenith angles the simplification of model must be considered as a serious source of uncertainty. Despite these facts, the results show improvement in the model estimates when shading is introduced, thus indicating the higher influence of terrain shading compared to the irradiance estimates errors. This is true especially for the sites with significant shading effect.

The other major source of error is the atmospheric parameterization as is used in the model for decomposition of global irradiance into its components and in the vertical

Please cite this article in press as: Ruiz-Arias, J.A. et al. Spatial disaggregation of satellite-derived irradiance using a high-resolution digital elevation model. Sol. Energy (2010), doi:10.1016/j.solener.2010.06.002

correction. Although a statistical method was used the influence of the errors in the decomposition are kept small because the radiation components are re-aggregated after applying the terrain corrections.

In addition to the previous error sources the uncertainty of ground measurements, especially for high zenith angles (cosine effect), may also negatively influence the presented results.

7. Conclusions

We have developed a disaggregation procedure to downscale the satellite-derived irradiance with original grid resolution of 3 arc min using the SRTM-3 DEM with 3 arc sec grid resolution. We focused on the influence of the terrain and the parameterization of the intra-grid cell variability of the solar radiation.

Overall, the described methodology has proven being able to reduce the initial mean bias error of the coarse satellite estimates caused by the insufficient terrain parameterization in complex terrain areas.

The relative importance of the terrain corrections changes along the day, season, and with the sky conditions. When the sky is cloudy, solar radiation is mostly diffuse and the shadowing and elevation corrections remain less important given the isotropic nature of the irradiance. However, sky-view fraction is important. Under cloudless skies, the relative weight of each correction changes during the day. At sunrise and sunset, when the sun altitude is low, shadowing correction may become the most important. As sun altitude increases, shaded terrain patches progressively disappear and changes in the vertical profile of irradiance are more important due to the increase of the differences in the optical path length. Under cloudless conditions, sky-view fraction correction is small but closely related to the atmospheric turbidity conditions, higher during the turbid seasons.

The reliability of the disaggregation procedure strongly depends on the specific point under consideration and is mainly driven by the terrain, therefore, by the quality and spatial resolution of the DEM. For the regions here evaluated, terrain disaggregation reduced the rMBE from around 2.3% to 0.4% (83% in relative terms). The rRMSE remained unaltered.

Acknowledgements

The authors would like to thank Jean Verdebout, Richard Perez, and Thomas Huld for inspiring discussions and valuable comments. This work was supported by the Spanish Ministry of Science and Technology (Project ENE2007-67849-C02-01), the Andalusian Ministry of Science and Technology (Project P07-RNM-02872), the JRC's FP7 framework program (Project 13106, SOLAREC), and by the Slovak Research and Development Agency (Contract VMSP-P-0042-07).

References

Abdel Wahab, M., El-Metwally, M., Hassan, R., Lefévre, M., Oumbe, A., Wald, L., 2008. Assessing surface solar irradiance in Northern Africa desert climate and its long-term variations from Meteosat images. International Journal of Remote Sensing 31 (1), 261–280.

Alsamamra, H., Ruiz-Arias, J.A., Pozo-Vázquez, D., Tovar-Pescador, J., 2009. A comparative analysis of ordinary and residual kriging techniques for mapping global solar radiation. Agricultural and Forest Meteorology 149, 1343–1357.

Cebecauer, T., Huld, T., Šúri, M., 2007. Using high-resolution digital elevation model for improved pv yield estimates. In: Proceedings of the 22nd European Photovoltaic Solar Energy Conference, Milano, Italy, pp. 3553–3557.

Dozier, J., Frew, J., 1990. Rapid calculation of terrain parameters for radiation modelling from digital elevation data. IEEE Transactions on Geoscience and Remote Sensing 28 (5), 963–969.

Dubayah, R., Loechel, S., 1997. Modeling topographic solar radiation using GOES data. Journal of Applied Meteorology 36, 141–154.

Dubayah, R., Dozier, J., Davis, F.W., 1989. The distribution of clear sky radiation over varying terrain. Proc. IGARSS 1989. IEEE, Vancouver, BC, Canada, pp. 885–888.

Dubayah, R., Dozier, J., Davis, F.W., 1990. Topographic distribution of clear sky radiation over the Konza Prairie, Kansas. Water Resources Research 26, 679–690.

Essery, R., Marks, D., 2007. Scaling and parametrization of clear-sky solar radiation over complex topography. Journal of Geophysical Research 112, D10122. doi:10.1029/2006JD007650.

Farr, T.G. et al., 2007. The shuttle radar topography mission. Reviews of Geophysics 45 (RG2004), 1–33, <http://www2.jpl.nasa.gov/srtm/>.

Gueymard, C.A., 1998. Turbidity determination from broadband irradiance measurements: a multicoefficent approach. Journal of Applied Meteorology 37, 414–435.

Hammer, A., Heinemann, D., Hoyer, C., Kuhlemann, R., Lorenz, E., Müller, R., Beyer, H.G., 2003. Solar energy assessmentnt using remote sensing technologies. Remote Sensing of Environment 86, 423–432.

Hofierka J., Huld T., Cebecauer T., Šúri M., 2007. Open source solar radiation tools for environmental and renewable energy applications. In: International Symposium on Environmental Software Systems, Prague, 2007.

Mayer, B., Kylling, A., 2005. Technical note: the libRadtran software package for radiative transfer calculations – description and examples of use. Atmospheric Chemistry and Physics 5, 1855–1877.

Moore, I.D., Norton, T.W., Williams, J.E., 1993. Modelling environmental heterogeneity in forested landscapes. Journal of Hydrology 150, 717–747.

Müller, R.W., Dagestad, K.F., Ineichen, P., Schroedter-Homscheidt, M., Cros, S., Dumortier, D., Kuhlemann, R., Olseth, J.A., Piernavieja, G., Reise, C., Wald, L., Heinemann, D., 2004. Rethinking satellite-based solar irradiance modelling. The SOLIS clear-sky module. Remote Sensing of Environment 91, 160–174.

Neteler, M., Mitasova, H., 2008. Open Source GIS: A GRASS GIS Approach, third ed. Springer Science + Business Media, New York, 406 p., <http://grass.osgeo.org/>.

Oliphant, A.J., Spronken-Smith, R.A., Sturman, A.P., Owens, I.F., 2003. Spatial variability of surface radiation fluxes in mountainous region. Journal of Applied Meteorology 42, 113–128.

Oumbe, A., Wald, L., 2010. A parameterisation of vertical profile of solar irradiance for correcting solar fluxes for changes in terrain elevation. In: Proceedings of the Earth Observation and Water Cycle Science Conference, 18-20 November, Frascati, Italy.

Perez, R., Stewart, R., Arbogast, C., Seals, R., Scott, J., 1986. An anisotropic hourly diffuse radiation model for sloping surfaces. Solar Energy 36 (6), 481–497.

Please cite this article in press as: Ruiz-Arias, J.A. et al. Spatial disaggregation of satellite-derived irradiance using a high-resolution digital elevation model. Sol. Energy (2010), doi:10.1016/j.solener.2010.06.002

Perez, R., Ineichen, P., Seals, R., Michalsky, J., Stewart, R., 1990a. Modeling daylight availability and irradiance components. Solar Energy 44, 271–289.

Perez, R., Ineichen, P., Seals, R., Zelenka, A., 1990b. Making full use of the clearness index for parameterizing hourly insolation conditions. Solar Energy 45 (2), 111–114.

Perez, R., Ineichen, P., Moore, K., Kmiecik, M., Chain, C., George, R., Vignola, F., 2002. A new operational satellite-to-irradiance model. Solar Energy 73 (5), 307–317.

Remund, J., Salvisberg, E., Kunz, S., 1998. On the generation of hourly shortwave radiation data on tilted surfaces. Solar Energy 62 (5), 331–344.

Rigollier, C., Bauer, O., Wald, L., 2000. On the clear sky model of the ESRA – European Solar Radiation Atlas – with respect to the Heliosat method. Solar Energy 68 (1), 33–48.

Rigollier, C., Lefèvre, M., Wald, L., 2004. The method Heliosat-2 for deriving shortwave solar radiation from satellite images. Solar Energy 77, 159–169.

Ruiz-Arias, J.A., Tovar-Pescador, J., Pozo-Vázquez, D., Alsamamra, H., 2009. A comparative study of DEM-based models to estimate solar radiation on mountainous terrains. International Journal of Geographical Information Science 23 (8), 1049–1076.

Ruiz-Arias, J.A., Tovar-Pescador, J., Pozo-Vázquez, D., Alsamamra, H., 2010. Proposal of a new regressive model for the hourly diffuse solar radiation under all sky conditions. Energy Conversion and Management 51, 881–893.

Siegel, R., Howell, J.R., 1981. Thermal Radiation Heat Transfer, second ed. McGraw-Hill, New York.

Šúri, M., Hofierka, J., 2004. A new GIS-based solar radiation model and its application for photovoltaic assessments. Transactions in GIS 8 (2), 175–190.

Tovar, J., Olmo, F.J., Alados-Arboledas, L., 1995. Local scale variability of solar radiation in a mountainous region. Journal of Applied Meteorology 34, 2316–2322.

Verdebout, J., 2000. A method to generate surface UV radiation maps over Europe using GOME, Meteosat, and ancillary geophysical data. Journal of Geophysical Research 105 (D4), 5049–5058.

Verdebout, J., 2004. A European satellite-derived UV climatology available for impact studies. Radiation Protection Dosimetry 111 (4), 407–411.

Wilson, J.P., Gallant, J.C., 2000. Secondary topographic attributes. In: Wilson, J.P., Gallant, J.C. (Eds.), Terrain Analysis: Principles and Applications. John Wiley & Sons.

Please cite this article in press as: Ruiz-Arias, J.A. et al. Spatial disaggregation of satellite-derived irradiance using a high-resolution digital elevation model. Sol. Energy (2010), doi:10.1016/j.solener.2010.06.002